Distributed Active Resonance Suppression in Hybrid DC Power Systems Under Unbalanced Load Conditions

Ehsan Jamshidpour, Babak Nahid-Mobarakeh, Philippe Poure, Serge Pierfederici, Farid Meibody-Tabar, Shahrokh Saadate

Distributed Active Resonance Suppression In Hybrid DC Power Systems Under Unbalanced Loads Conditions

E. Jamshidpour, B. Nahid-Mobarakeh, P. Poure, S. Pierfederici, F. Meibody-Tabar, S. Saadate

Abstract **– Power electronics based Hybrid DC Power Systems (HDCPSs) are increasingly used in many industrial applications such as land, sea and air vehicles. In these systems, small DC-link and LC filter capacitors are of great interest for weight saving. However, this may lead to either increase unstable oscillations, because of constant power load with negative dynamic impedance, or produce resonance in unbalanced loads conditions. In this paper, a distributed active oscillation suppression approach is presented. It is based on the analytical study of the linearized model of the studied system around the operating point. The studied system consists of one main DC source and one storage element supplying two loads: a Permanent Magnet Synchronous Motor (PMSM) connected to the DC-link by a voltage source inverter and a resistive load supplied by a DC/DC converter. The proposed approach is particularly used to overcome the resonance under unbalanced loads conditions and allows reducing DC-link and LC filter capacitors for weight saving. Simulations and experimentations are carried out which confirm the validity of the proposed approach.**

Keywords **– Active Resonance Suppression, Stability, Hybrid DC Power System (HDCPS), Constant Power Load (CPL), Unbalanced Load, DC-link Capacitor.**

Ehsan Jamshidpour (*ehsan.jamshidpour@green.uhp-nancy.fr*), Babak Nahid-Mobarakeh, Serge Pierfederici, Farid Meibody-Tabar and Shahrokh Saadate are with "Groupe de Recherche en Electronique et en Electrotechnique de Nancy" (GREEN), 2 av de la foret de Haye, 54516 Vandoeuvre-les-Nancy, France. Philippe Poure is with "Laboratoire d'Instrumentation Electronique de Nancy" (LIEN), Faculté des Sciences et Technologies – BP70239 - 54506 Vandoeuvre-les-Nancy, France.

I. Introduction

The increasing use of electrical actuators in industrial applications results in more complex electrical distribution systems. In this case, power electronics based Hybrid DC Power Systems (HDCPSs) are excellent candidates. They can offer excellent load regulation and transient performance, and with proper architecture a high degree of fault tolerance.

Unfortunately power electronics based HDCPSs have also some disadvantages which may lead system to instability. For example, in typical applications such as electrical ships, submarines, aircrafts, space crafts and vehicles, small DC-link and filter capacitors are of great interest for weight reduction. As a consequence, reducing the DC-link capacitance decreases the system damping ratio and increases the instability risk due to interactions between subsystems [1], [2].

Also, when power electronics converters or motor drives are tightly controlled, they can be considered as Constant Power Loads (CPLs) in short time scales [3]. CPLs have negative impedance characteristics at the input terminals during dynamics. This behavior has a destabilizing effect, so called negative impedance instability. Therefore, CPLs interaction with other devices may affect the stability and the dynamic of the HDCPS [3]-[6].

On the other hand, some stable oscillations could be produced under unbalanced load conditions. There is a risk of resonance when oscillation frequency is close to the system natural frequency. Typical examples of unbalanced load conditions are oscillatory speed due to external operating conditions and/or ripples on the motor torque caused by an unbalanced mechanical load or a mechanical/electrical fault. Such a resonance risks to be propagated to the whole HDCPS, making oscillate its voltages and currents. Contrarily to the instability risk due to tightly controlled loads, the resonance may produce stable oscillations with significant magnitudes. One solution to reduce the risk of resonance is increasing capacitive components in the network, so called passive resonance suppression [7].

Here, the proposed active resonance suppression approach provides distributed active compensators which reduce significantly the risk of resonance in a HDCPS while DC-link and LC filters capacitors are minimized. This approach has three advantages. First, the stability margin of the system is increased under normal conditions. Second, by choosing proper compensator parameters for each load, it is possible to reduce drastically the effects of unbalanced loads and so, the risk of resonance. Third, the size of the DC-link and LC filter capacitors could be

reduced without decreasing stability margins and resonance suppression capabilities. In the following, the proposed approach for a HDCPS, consisting of a main DC source, an ultracapacitor (UC) and two tightly controlled loads under normal and unbalanced conditions is developed.

This paper is organized in six sections. The studied HDCPS modeling and control strategy is presented in the following section. Then, in Section III, the proposed distributed active resonance suppression approach is detailed. In Sections IV and V, simulation and experimental results are presented which confirm the validity of the proposed method. The last section provides some remarks and conclusions.

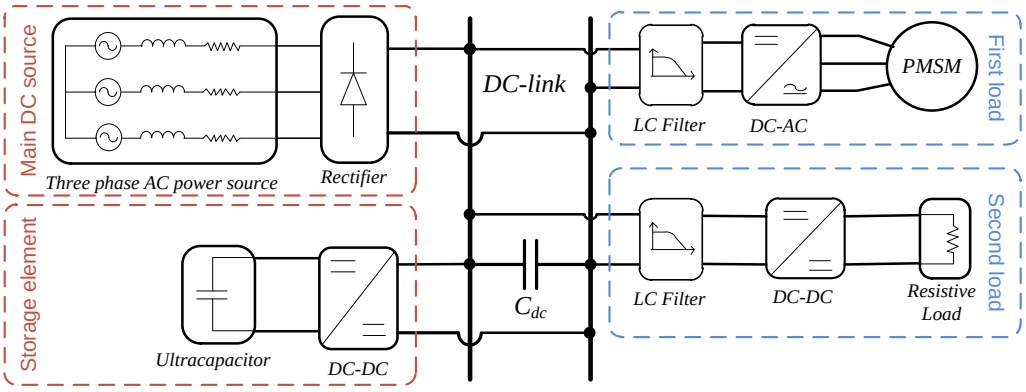

Fig. 1. Scheme of the studied HDCPS.

II. HDCPS Modeling and Control Strategy

II.1. HDCPS Modeling

Fig. 1 shows the HDCPS studied in this paper which consists of a main DC source, a storage element and two loads. In a HDCPSs and more particularly in transportation systems, the voltage source is placed far from the loads and a long cable may be used between the source and the DC-link [1]. As a result, the inductance and resistance of the cable are included in this modeling, as shown in Fig. 2 (R_e and L_e). The storage element is an UC connected to the DC-link through a bidirectional DC-DC converter. It is modeled by a capacitor (C_{uc}), an equivalent parallel resistance (R_{Puc}), converter inductance L_{uc} and equivalent resistance R_{uc} (sum of series resistor of UC and converter resistor) [8], [9]. The DC-link capacitor C_{dc} acts as buffer for DC-link voltage (v_{dc}).

Two loads are supplied through the LC filters and power electronic converters. For the LC filters, L_{f1}, R_{f1} and L_{f2}, R_{f2} stand for the filter and cables inductances, since C_{f1} and C_{f2} are the filters capacitors. The first load is a non-salient Permanent Magnet Synchronous Motor (PMSM), supplied by a PWM controlled DC-AC converter. The second one is a resistive load connected to the DC-link through a PWM controlled DC-DC converter. The loads powers are noted P_1 and P_2. As precised before, when a converter tightly regulates its output, then it behaves as a Constant Power Load (CPL) [3], [4], [10]. So, in short time scale, the loads and converters can be considered as current sources, as shown in Fig. 2. In the proposed modeling, the power switches are modeled by ideal ones.

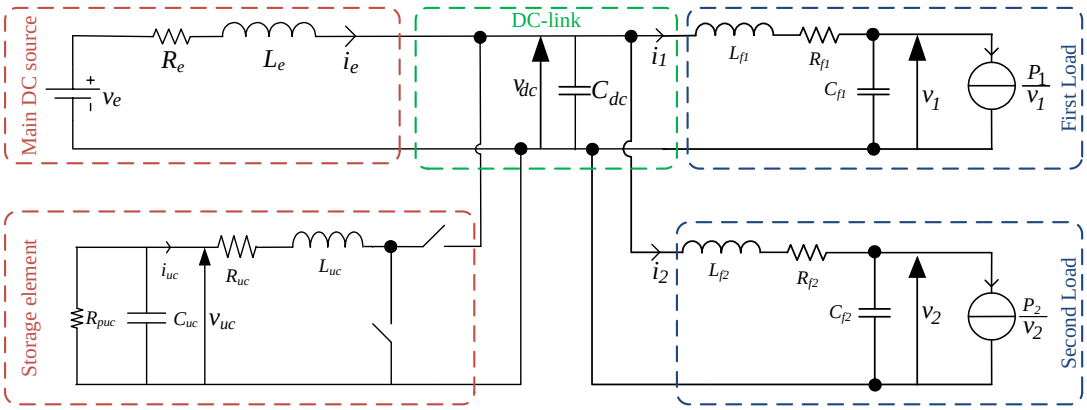

Fig. 2.The HDCPS modeling.

II.2. Control system strategy

To control the HDCPS, we consider an individual control for each load and a global control loop for system's energy management. Since the power sources in the HDCPSs have slow dynamic, a fast load variation may lead to a high under/over voltage in the DC-link and affects the controllability of the system. Therefore, applying a suitable control on the UC allows controlling efficiently DC-link voltage during fast load variations.

Some methods to control and optimize energy management in DC network have been presented in the literature [1], [5], [6], [11]-[14]. In this paper, Proportional Integral (PI) controllers are used to manage DC-link stored energy ($\epsilon_{dc} = \frac{1}{2} C_{dc} v_{dc}^2$) by the UC's output current (i_{uc}) control. In fact, by controlling ϵ_{dc}, the DC-link voltage can be indirectly controlled. A classical vector control is used in the torque (or current) control loop of the PMSM. The power of resistive load is tightly controlled by a PI controller. Also, for safety and dynamic considerations, the

UC voltage is controlled between 50% and 100% of its maximum rated voltage to avoid damages and saturation of the DC-DC converter. Also, the converter of the UC is usually primarily controlled by inner current-regulation loop.

II.3. System's Mathematical Modeling and Stability study

The HDCPS given in Fig.2, completed by associated controls, is presented in Fig. 3. This system can be modeled by differential equations provided below (1) (without compensation).

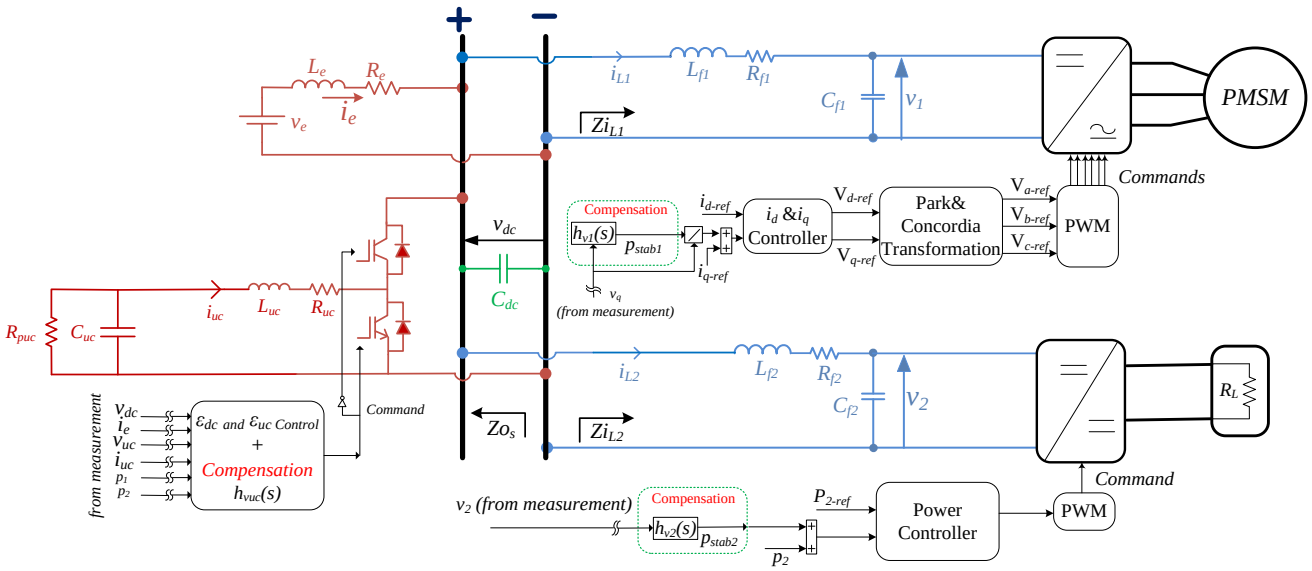

Fig. 3. Block diagram of the control loops and compensation blocks.

$$\begin{cases} \frac{dv_1}{dt} = \frac{1}{C_{f1}}\left(i_1 - \frac{p_1}{v_1}\right) \\ \frac{dv_2}{dt} = \frac{1}{C_{f2}}\left(i_2 - \frac{p_2}{v_2}\right) \\ \frac{dv_{uc}}{dt} = \frac{-1}{C_{uc}R_{puc}}\left(i_{uc}R_{puc} + v_{uc}\right) \\ \frac{dv_{dc}}{dt} = \frac{-1}{C_{dc}}\left(i_1 + i_2 - i_e - i_{uc}(1 - d_{uc})\right) \\ \frac{di_{uc}}{dt} = \frac{1}{L_{uc}}\left(v_{uc} - R_{uc}i_{uc} - v_{dc}(1 - d_{uc})\right) \\ \frac{di_e}{dt} = \frac{-1}{L_e}(v_{dc} - v_e + R_e i_e) \\ \frac{di_1}{dt} = \frac{1}{L_{f1}}\left(v_{dc} - v_1 - R_{f1}i_1\right) \\ \frac{di_2}{dt} = \frac{1}{L_{f2}}\left(v_{dc} - v_2 - R_{f2}i_2\right) \\ \frac{dS_{iuc}}{dt} = i_{ucref} - i_{uc} \\ \frac{dS_{\epsilon dc}}{dt} = \frac{1}{2}C_{dc}\left(v_{dcref}^2 - v_{dc}^2\right) \end{cases} \quad (1)$$

where d_{uc} stands for the UC's DC/DC converter duty cycle ($0 \leq d_{uc} \leq 1$). To determine the operating points, the left side of (1) is forced to zero. Then, the operating points are determined, indicted below by "0". To simplify the use of this model for stability study, following state variables are introduced (2):

$$\begin{cases} v_1(t) = V_{10} + x_1(t) \\ v_2(t) = V_{20} + x_2(t) \\ v_{uc}(t) = V_{uc0} + x_3(t) \\ v_{dc}(t) = V_{dc0} + x_4(t) \\ i_{uc}(t) = I_{uc0} + x_5(t) \\ i_e(t) = I_{e0} + x_6(t) \\ i_1(t) = I_{10} + x_7(t) \\ i_2(t) = I_{20} + x_8(t) \\ s_{iuc}(t) = S_{iuc0} + x_9(t) \\ s_{\epsilon dc}(t) = S_{\epsilon dc0} + x_{10}(t) \end{cases} \quad (2)$$

Then the state variables vector is given in (3).

$$X = (x_1, x_2, x_3, x_4, x_5, x_6, x_7, x_8, x_9, x_{10})^T \quad (3)$$

After substituting (2) to (1), we find a space state model as presented by (4).

$$\frac{d}{dt}\begin{bmatrix} x_1 \\ x_2 \\ x_3 \\ x_4 \\ x_5 \\ x_6 \\ x_7 \\ x_8 \\ x_9 \\ x_{10} \end{bmatrix} = \begin{bmatrix} \frac{\left(+I_{10} - \frac{P_{10}}{V_{10}+x_1}\right)}{C_{f1}} \\ \frac{\left(x_8 + I_{20} - \frac{P_{20}}{V_{20}+x_2}\right)}{C_{f2}} \\ -\frac{\left((I_{uc0}+x_5)R_{puc} + V_{uc0} + x_3\right)}{C_{uc}R_{puc}} \\ -\frac{I_{10+}I_{20} - I_{e0} - x_6 + x_7 + x_8 - (I_{uc0}+x_5)A_2}{C_{dc}} \\ \frac{V_{uc0} + x_3 - R_{uc}(I_{uc0}+x_5) - (V_{dc0}+x_4)A_2}{L_{uc}} \\ -\frac{V_{dc0} + x_4 - V_e + R_e(I_{e0}+x_6)}{L_e} \\ \frac{V_{dc0} + x_4 - V_{10} - x_1 - R_{f1}(x_7 + I_{10})}{L_{f1}} \\ \frac{V_{dc0} + x_4 - V_{20} - x_2 - R_{f2}(x_8 + I_{20})}{L_{f2}} \\ -x_5 - I_{uc0} + \frac{K_{I\epsilon dc}(x_{10} + S_{\epsilon dc0}) + \frac{C_{dc}K_{P\epsilon dc}A_1}{2}}{V_{uc0}+x_3} \\ A_1 \end{bmatrix} \quad (4)$$

Note that p_1 and p_2 (Fig. 3) are supposed to be constant. K_{Puc}, $K_{P\epsilon dc}$, $K_{I\epsilon dc}$, K_{Piuc} and K_{Iiuc} are the parameters of the PI controllers. The parameters A_1 and A_2 (4) are defined below, by (5) and (6).

$$A_1 = \frac{1}{2}\left(V_{dcref0} - \frac{C_{uc}K_{Puc}\left(V_{ucref}^2 - (V_{uc0}+x_3)^2\right)}{2}\right)^2 - (V_{dc0}+x_4)^2 \quad (5)$$

$$A_2 = -x_5 - I_{uc0} + \frac{K_{I\epsilon dc}(S_{\epsilon dc0} + x_{10}) + \frac{C_{dc}K_{P\epsilon dc}A_1}{2}}{V_{uc0}+x_3} \quad (6)$$

Because of CPLs, this model is nonlinear. To simplify the stability study, a linearized model around the operating point of the system is used. To evaluate the impact of p_1 and p_2 on the local stability of the system, the eigenvalues of Jacobian matrix of the state equations (4) are determined. To find the stability limit of the system, for each P_1 ϵ[0, 1000], P_2 has been modified from 0 to 1000 and the eigenvalues of Jacobian matrix are calculated. As soon as the real part of any eigenvalue becomes positive, the system is passed beyond the stability limit. By repeating this operation for each p_1, we can determine the stability limit of the system. The used parameters are shown in table I which correspond to the system shown in Fig. 3 (without compensation); the stability limit of the system is obtained and is shown in Fig. 4. It should be noted that particularly the inductances are chosen important enough,

then unstable oscillation occur at relatively low powers in order to avoid damaging of the experimental bench realized for this study.

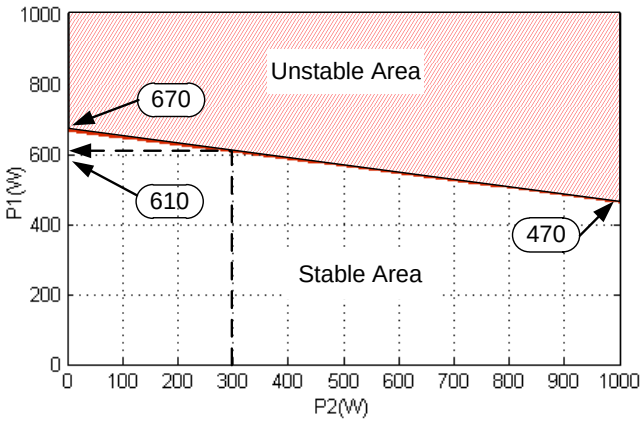

Fig. 4. Stable and unstable regions as a function of p_1 and p_2

TABLE I
SIMULATION AND EXPERIMENTAL SYSTEM PARAMETERS

Main DC Power Source			
V_e=200 V	Le=20 mH	Re=0.5 Ω	
Stotage Element (UC)			
C_{uc}=165 F	L_{uc}=20 mH	R_{uc}=0.5 Ω	R_{Puc}=10 KΩ
First Load Filter			
C_{f1}= 500μF	L_{f1}=39.5 mH	R_{f1}=14 Ω	R_L=14Ω
Second Load Filter			
C_{f2}= 1100μF	L_{f2}=20 mH	R_{f2}=0.7 Ω	

III. Distributed Active Oscillation Suppression

The asymptotic stability of the system is also threatened by the risk of resonance. Indeed, there are resonant modes in HDCPSs because of the presence of poorly damped LC filters. If these modes are excited, stable oscillations will appear and will propagate to the entire system. This excitation may come from the main source, the storage elements or unbalanced load conditions. Filter damping can be improved by passive manner [7]. In applications where light and small capacitances are desired, the risk of resonance is more important. In addition, the ageing of capacitors increases also this risk.

To improve the performances of the studied HDCPS for resonance aspects, a decentralized linear compensator is provided; i.e. an independent oscillation suppression block is considered for each load and each controlled source (storage element in our case), as shown in Fig. 3.

The proposed active oscillation suppression block is composed of a proportional compensator followed by a band-pass filter. This filter eliminates measurement noises and preserves a good behavior for the system at very low frequencies. The transfer function for $h_{v_j}(s)$ is as follows (Fig. 3):

$$h_{v_j}(s) = K_j \frac{2\xi\omega_{f_j}s}{s^2 + 2\xi\omega_{f_j}s + \omega_{f_j}^2} \quad j = 1, 2 \; and \; uc \tag{7}$$

where ω_{f_j} is chosen equal to the resonant frequency of the input LC filter of each load and K_j is a proportional gain to be set to meet the local stability requirements and the constraints on the magnitude of the resonance peak. These requirements are often given in terms of minimum Gain Margin (GM), Phase Margin (PM) and attenuation at the resonance frequency. The bandwidth of h_{v_j}, fixed by ξ, should be sufficiently large to cover all resonance frequencies of the network. The output of the oscillation suppression block is a stabilizing power (8) which should be added to the load power reference (9):

$$\begin{cases} p_{1_{stab}} = h_{v1}(s) \cdot \tilde{v}_1 \\ p_{2_{stab}} = h_{v2}(s) \cdot \tilde{v}_2 \\ p_{uc_{stab}} = h_{vuc}(s) \cdot \tilde{v}_{uc} \end{cases} \tag{8}$$

Then:

$$\begin{cases} p_1 = P_{10} + p_{1_{stab}} \\ p_2 = P_{20} + p_{2_{stab}} \\ p_{uc} = P_{uc0} + p_{uc_{stab}} \end{cases} \tag{9}$$

In practice these stabilizing powers are generated depending on the nature of each load. For the PMSM (first load), p_{1stab} is generated by using the quadrature axis current and voltage (i_q and v_q) of the machine. For the UC and the resistive load, p_{2stab} is generated by either the current or power control loop.

First, for stabilization purposes, different techniques may be applied to determine the proportional gain K_j for satisfying the local stability requirements. One of them is based on the fact that the local stability around an operating point of two cascade converters depends on the poles of the transfer function $1/(1+T_m)$, where

T_m=$Z_o(s)/Z_i(s)$ with $Z_o(s)$ the output impedance of the source(s) side and $Z_i(s)$ the input impedance of the load(s) side (see Fig. 3) [15], [16]. The oscillation suppression blocks modify the input impedance $Z_i(s)$ and improve the stability margins. To apply this design approach, we have to determine the input impedance of each load as a function of K_j. Then, the stability margins can be obtained from the well known linear analysis tools as Bode or Nyquist plots of T_m. Here, we give only the Nyquist plot of T_m for the first load (PMSM) for P_{10}=750W and P_{20}=850W (an unstable operating point according to Fig. 4) when K_1 varies between 0 and 100 (see Fig. 5). The system parameters are those given in Table I. From Fig. 6, the system is unstable when K_1=*0*. It can also be deduced from this figure that K_1 *around 10* is a good choice for the stability margins. Indeed, the stability margins are maximized with K_1=*8.8:* GM=16.9 *dB* and PM=68°.

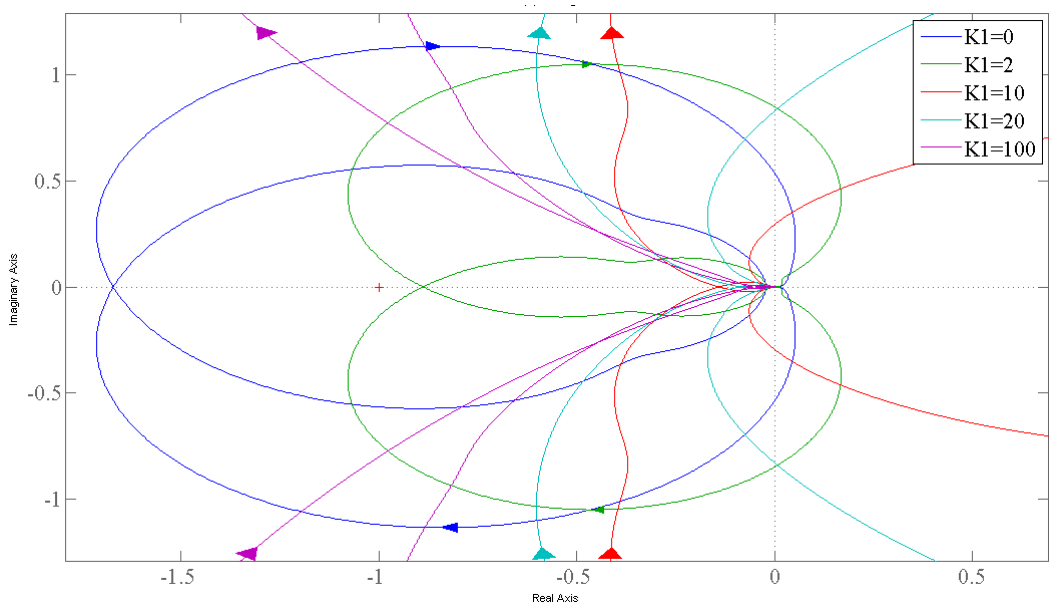

Fig. 5. Impact of K_1 on the system's stability.

Second, for resonance suppression purposes, the design procedure is clearly different. It is obvious that the proportional gain K_j affects also the resonance peaks in all transfer functions $\tilde{v}_i/\tilde{p}_i$. For example, Fig.6. shows the impact of K_1 on the transfer function $\tilde{v}_1/\tilde{p}_1$ for $P_{10} = 450W$ and $P_{20} = 800W$ when K_1 varies between 0 and 100. It should be noted that this operating point is stable (see Fig. 4), but as it will be shown in the simulation and experimental results, significant oscillations appear on the DC-link when this latter is excited at its resonance frequency by one of the loads. As it can be seen in Fig. 6 for the first load, the resonance peak is significantly

reduced by the resonance suppression block. For example, if the minimum required attenuation at 224 *rad/s* is 20 *dB*, K_1 should be greater than 10.3. If we set K_1 to 10.3, the stability margins are still satisfactory (GM=17.1 *dB* and PM=67°). It can be also noted that from resonance suppression point of view, the best choice of K_1 is obviously the biggest one (K_1=100 in Fig. 6). However, this choice reduces the stability margins (see Fig.5). So, a good trade-off between resonance suppression and stability margins on one hand and another trade-off between resonance suppression and load performances on the other hand have to be found. Else, the passive elements should be increased to improve the resonance suppression in a passive manner.

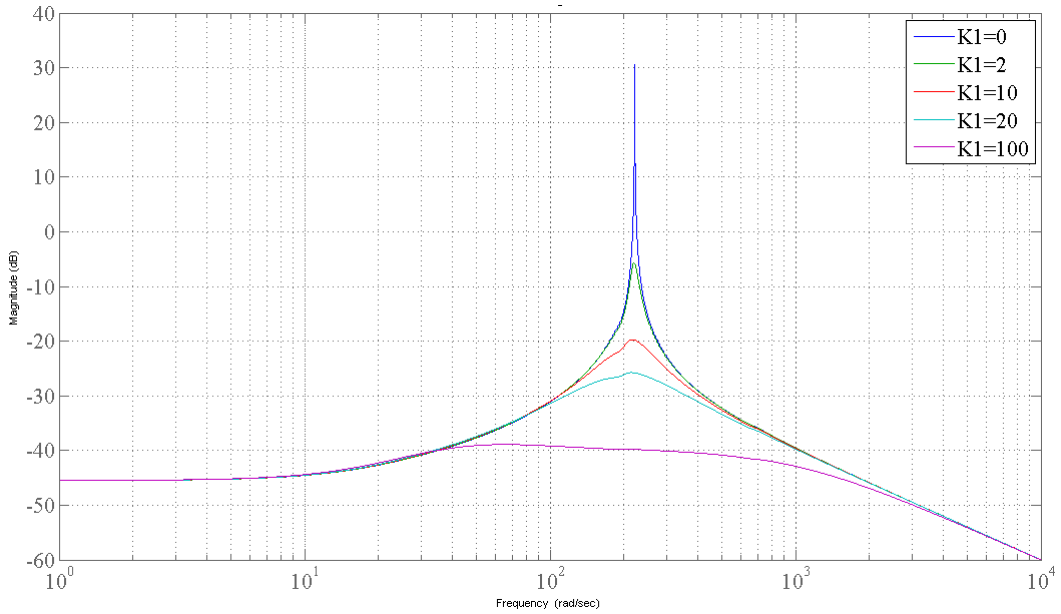

Fig. 6. Impact of K_1 on the resonance peak of the transfer function $\tilde{v}_1/\tilde{p}_1$.

This design procedure is applied to all compensator blocks. For our application, K_2 is fixed at 6.6 to get 20*dB* attenuation on the resonance peak of the transfer function $\tilde{v}_2/\tilde{p}_2$. The compensator parameters are given in Table II.

It can be proved, by repeating the process applied to find stability margin of the system without compensation blocks (Fig. 4), that the same stability margins and resonance peak attenuation can be achieved if C_{f1} and C_{f2} are respectively 4.6 and 3.7 times higher than those given in Table I. So, the use of the proposed active resonance

suppression blocks allows reducing these capacitances without significantly affecting the load dynamic as discussed in the next section.

It should be noted that in recent publications, [15] and [17], the transfer function (7) is proposed to be used to stabilize a power system formed by a source and a CPL under normal conditions. In this paper, we applied that to the studied HDCPS with two sources and two CPLs. We emphasize on its properties on resonance suppression in the HDCPS by attenuating the resonance peak in transfer function $\tilde{v}_i/\tilde{p}_i$ under unbalanced load conditions.

IV. Simulation Results

The simulations using MATLAB - Simulink with the parameters of Tables I and II are carried out. In Fig. 8, first at *t=0.5 s* the second load with p_2=300W is connected to the system and then at *t=1s*, the first load with p_1=500W is connected. In these conditions, the system remains stable. At *t=4s*, p_1 increased up to 620W and the system becomes unstable (confirming the limit of Fig. 4). Then, the compensation blocks (with parameters given in Table II) are activated at *t=8s* and the system comes back to a stable state. At *t=9s*, p_1 and p_2 are increased respectively to 1300W and 600W without affecting the stability of the system. Simulation results show that without changing the value of the passive elements in the system, the stability limit is doubled.

TABLE III
PARAMETERS OF THE COMPENSATION BLOCK

K_1=10.3	K_2=6.6	K_{uc}=0.5 Ω
ω_{f1}=225 rad/s	ω_{f2}=213 rad/s	ω_{fuc}=215 rad/s
ξ_1=0.7	ξ_2=0.7	ξ_{uc}=0.7

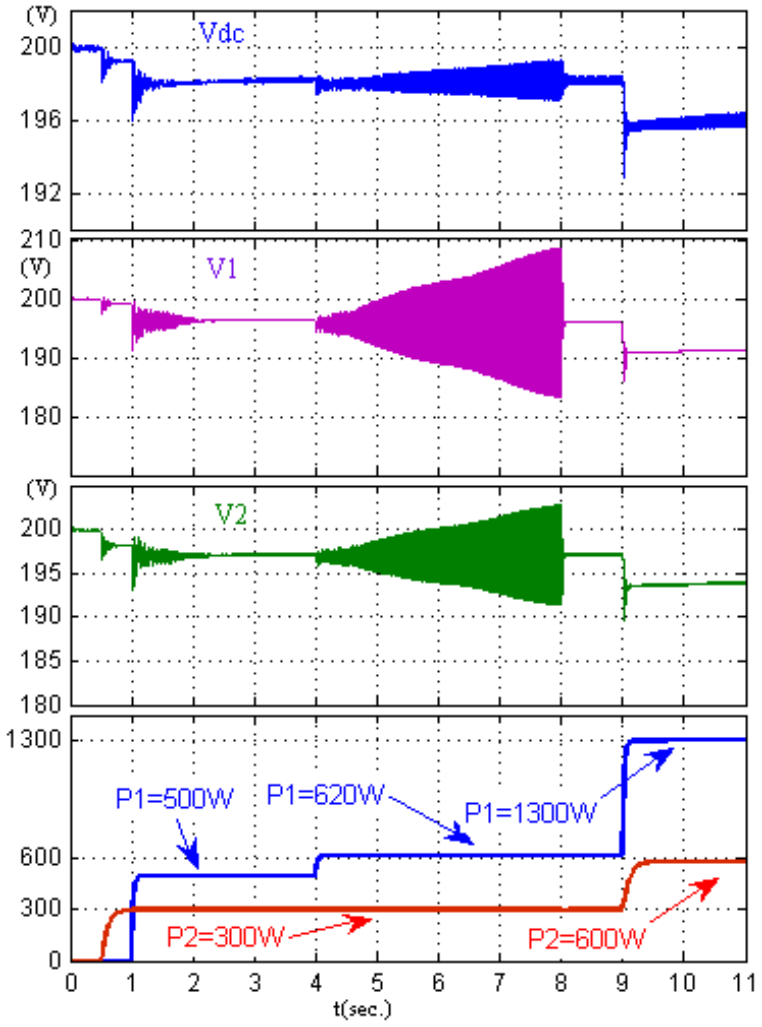

Fig. 7. Simulation results without and with the compensation blocks.

As mentioned in the previous section, the asymptotic stability of the system is also threatened by the risk of resonance. Particularly, variable speed drives are widely used in typical HDCPSs. They have potential to excite the resonance modes because of the risk of oscillating mechanical loads or electrical/mechanical imbalances. In these cases, low frequency harmonics may appear in the motor torque, in the back-EMF or in the stator voltages and currents [8]. To realize this condition, we superpose a low frequency oscillating component on the absorbed power of the first load (1). A small signal analysis can be performed by plotting the magnitude diagram of the transfer function ($\tilde{v}_1/\tilde{p}_1$). As it can be seen in Fig.8, there is a resonance peak at 224 *rad/s* with a magnitude of 30 *dB* for p_1=450W and p_2=800W. It should be noted that this operating point is stable according to Fig.4. In fact, the resonance peak grows up rapidly when the operating point approaches the unstable area (see Fig.8). This can be

verified by simulation. Fig. 9 shows the simulation results in which P_2=300W and P_1=*450W* plus a 2.2 percent sinusoidal oscillation at resonance frequency, i.e. P_1=*450+10 sin(224t)* for t< 4*s*. While small oscillations appear on the DC-link voltage (v_{dc}) and on some other variables such as v_1 and v_2 , the system remains still stable. At t=4s, the operating point is moved to p_2=800W (Fig. 9). As it was explained, the amplitude of these oscillations becomes important and we fail to control the system which becomes unstable.

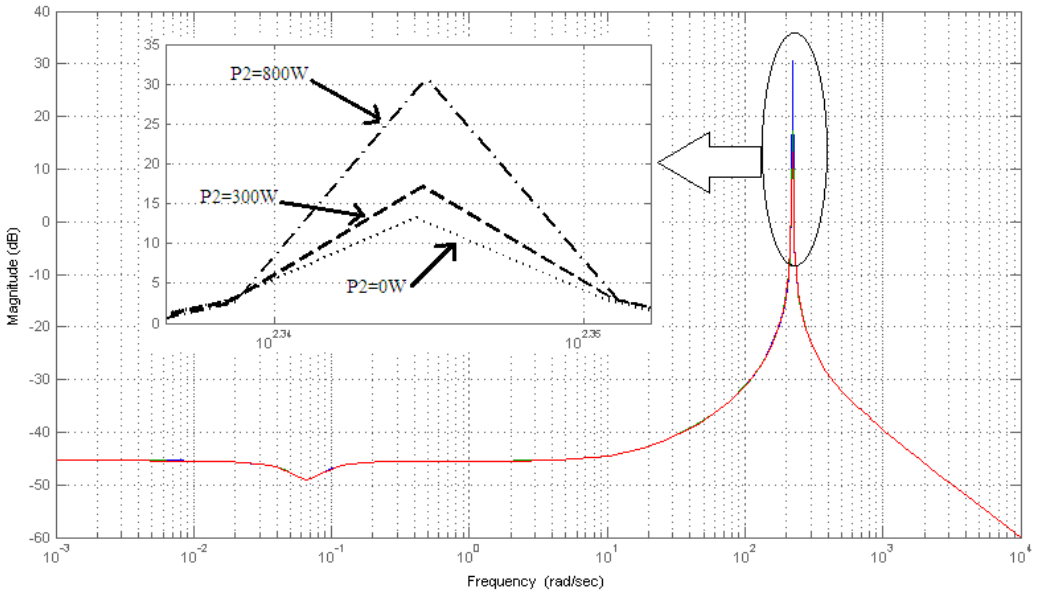

Fig. 8. Bode diagram of the transfer function $\tilde{v}_1/\tilde{p}_1$ for $p_1 = 450W$.

It is notable that by plotting other transfer functions ($\tilde{v}_i/\tilde{p}_i$), it can be easily shown that the worst resonance peak for $\tilde{v}_i$ occurs when the source of oscillations is $\tilde{p}_i$.

To verify the efficiency of the proposed active resonance suppression method, the system is simulated with enabled resonance suppression blocks. As shown in Fig. 10, the operating point of the system is p_1=550W and p_2=800W. At *t=4s* a sinusoidal oscillation (*10 sin(224t)*) is appeared on p_1. Unlike the previous simulation, the system remains stable. These simulation results show the efficiency of the proposed active resonance suppression method to reduce the resonance risk.

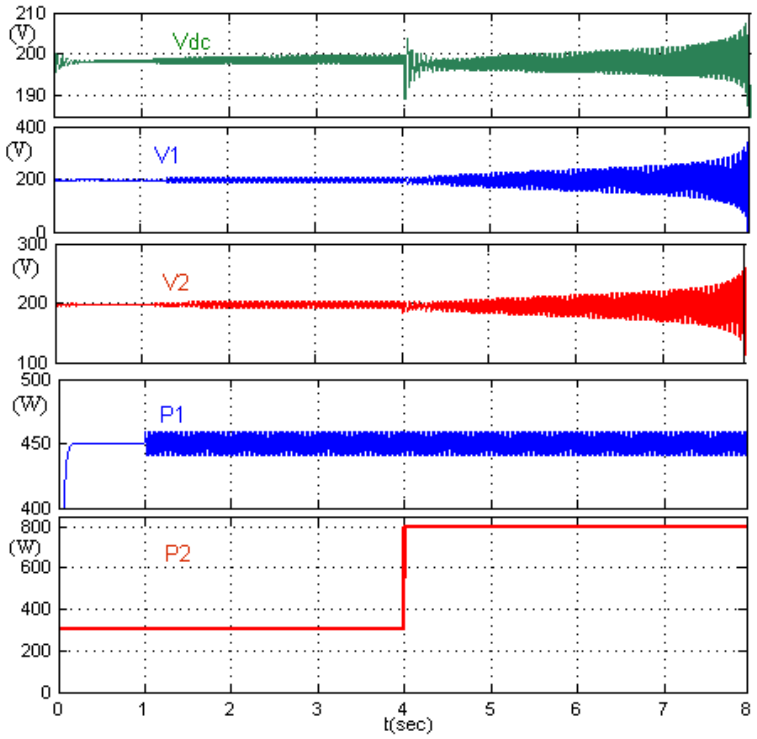

Fig. 10. Simulation results under resonance conditions at 224 *rad/s*.

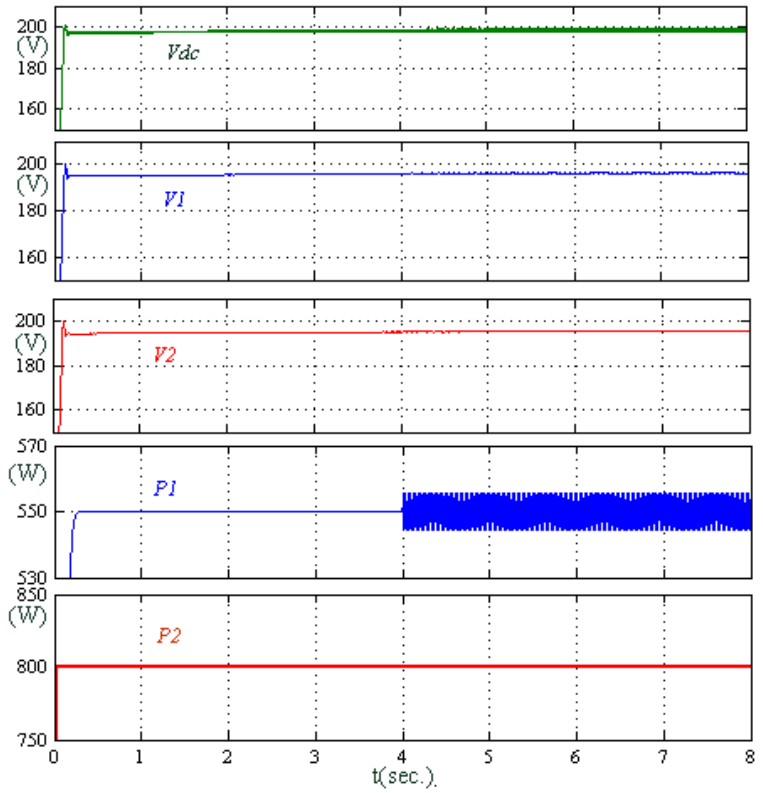

Fig. 9. Simulation results when a resonance mode is excited with $\tilde{p}_1$ (active resonance suppression blocks are enabled).

V. Experimental Results

Some experiments were carried out to validate the performances of the proposed distributed active resonance suppression approach. The experimental bench realized for this study is shown in Fig. 11. A dSpace DS1004 card was implemented for a real-time control of the system. The sampling period is 100 µs. The switching frequency of the inverter is 10 kHz. The parameters of this bench are the same that we used in simulations and are given in Tables I and II. The measurements are realized by sufficiently high bandwidth sensors (>150 kHz) and sampled either by a 20-MHz oscilloscope or by the digital control card. A programmable power source is used as the main DC source and an UC (Maxwel BMOD0165) is used as the storage element. A PMSM drive and a resistive load are tightly controlled by converters and are connected through their LC filters to the DC-link.

Fig. 11. Experimental bench.

Figs. 12 to 14 show the efficiency of the proposed distributed active resonance suppression when one of the resonance modes of the system is excited. In Fig. 12, the system is in stable region ($p_1 = 550W$ and $p_2 = 300W$). As explained before, p_1 is controlled by i_q. To make an unbalanced load condition, a sinusoidal oscillation is added in the reference of the i_q , therefore a small amplitude oscillation ($\pm 20W$) with a frequency close to the resonance frequency is appeared on p_1. To show this oscillation, a zoom of Fig. 12 is provided in Fig.13. In Fig. 13, it can be clearly seen that some oscillations appear on the voltages v_1 and v_2. The magnitude of these oscillations increases

until the system is no more controllable. The only way to suppress these oscillations is to enable the compensation blocks. As depicted in Fig. 14, when the compensation blocks are enabled, the system comes back into the stable mode very fast.

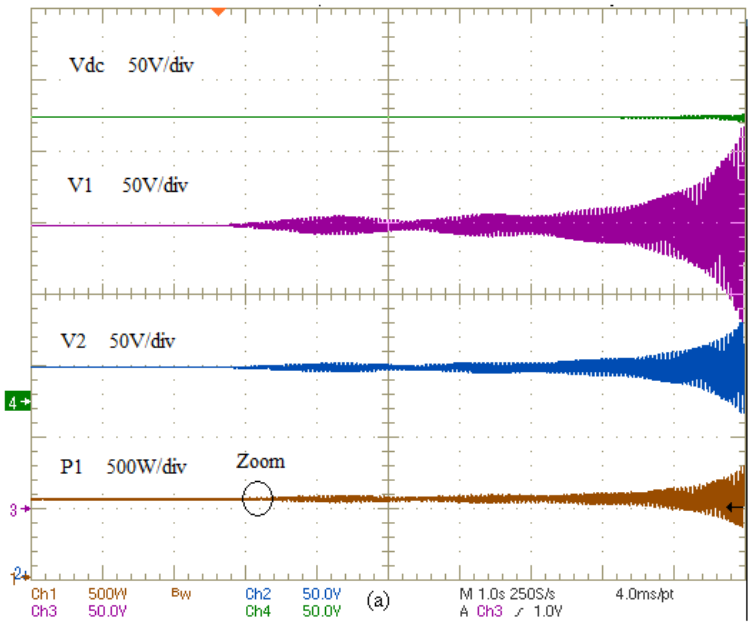

Fig. 12 Instability caused by oscillation under unbalanced load (p_1=450W, p_2=300W without compensation).

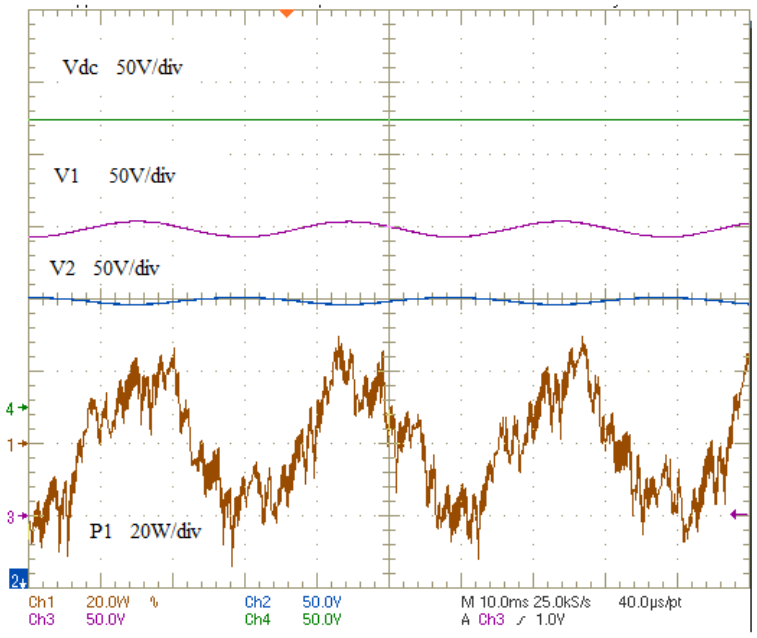

Fig. 13 Zoom of Fig. 12 showing the oscillation in stable region (p_1=450W, p_2=300W, without compensation).

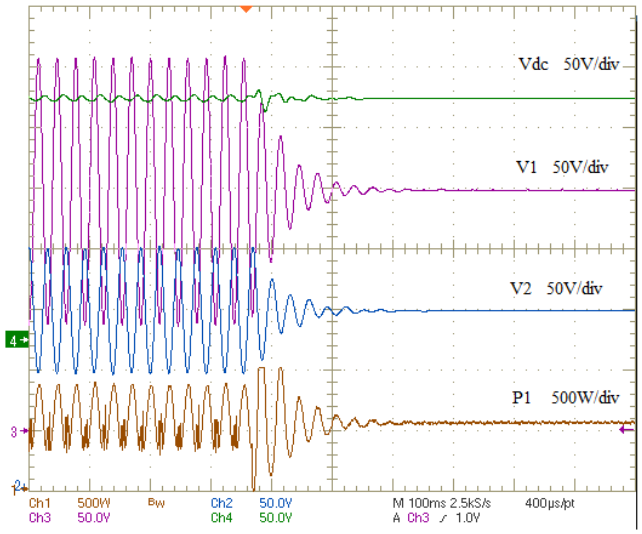

Fig. 14. Effect of enabling compensation blocks during instability caused by resonance.

More, as discussed in the previous sections, the active oscillation suppression approach also increases the stability margin of the system. Indeed, in Fig. 15, the compensation blocks are enabled and the system is stable for $P_1=732W$ and $P_2=300W$, while according to Fig.4, these powers correspond to an unstable operating of system. When the compensation blocks are disabled the system lost its stability. This means that the compensation blocks stabilize the system under normal condition of CPLs.

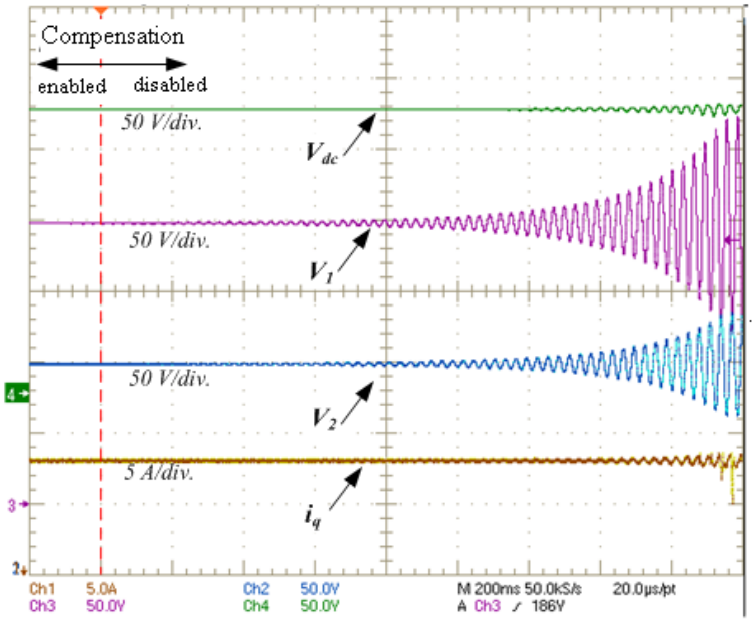

Fig. 15 Effect of compensation blocks on stability (p_1=732W; p_2=300W compensation blocks pass from enabled to disabled)

VI. Summary/Conclusion

In this paper, a distributed active resonance suppression approach for HDCPSs is proposed. Transportation systems are mainly concerned by this study because of load and source converters interaction, small DC-link and LC filter capacitors utilization and resonance which could be produced by actuators. The emphasis was put on the resonance modes which may be excited by oscillating loads, faulty loads or unbalanced loads supplied by the HDCPS. The proposed distributed active resonance suppression approach is based on providing an active compensation block for each load and controlled source. Here, this block is realized by a band-pass filter and a proportional compensator. A design procedure was proposed for determining the resonance suppression block's parameters. It was shown that not only these blocks suppress stable oscillations due to resonance modes of the system but also they improve the stability margins of the whole system. The simulation and experimental results confirmed the validity and efficiency of the proposed approach.

VII. References

[1] D. Marx, P. Magne, B. Nahid-Mobarakeh, S. Pierfederici, and B. Davat, "Large signal stability analysis tools in DC power systems with constant power loads and variable power loads- A Review," IEEE *Trans. Power Electron.*, vol. 27, No.4, pp. 1773-1787, Apr. 2012.

[2] W. J. Lee and S. K. Sul, "DC-link voltage stabilization for reduced DC-link capacitor inverter," in *IEEE Energy Conversion Congress and Exposition, ECCE 2009* , pp. 1740-1744, 2009, pp. 1740-1744.

[3] A. M. Rahimi, G. A. Williamson, and A. Emadi, "Loop-cancellation technique: A novel nonlinear feedback to overcome the destabilizing effect of constant-power loads," *IEEE Trans. on Veh. Technol.*, vol. 59, pp. 650-661, 2010.

[4] A. Emadi, A. Khaligh, C. H. Rivetta, and G. A. Williamson, "Constant power loads and negative impedance instability in automotive systems: Definition, modeling, stability, and control of power electronic converters and motor drives," *IEEE Trans. on Veh. Technol.*, vol. 55, No. 4, pp. 1112 - 1125, Jul. 2006.

[5] P. Magne, B. Nahid-Mobarakeh, and S. Pierfederici, "General Active Global Stablization of multiloads DC-power networks," *IEEE Trans. Power Electron.*, vol. 27, No.a, pp. 1788-1798, Apr. 2012.

[6] T. Duong, H. Zhou, and A. M. Khambadkone, "A simple design of DC power system with multiple source-side converters to operate stably under constant power load," *2nd IEEE International Sym. on Power Electron. for Distributed Generation Systems (PEDG),* pp. 520-525. Jun. 2010

[7] M. Cespedes, L. Xing, and J. Sun, "Constant-power load system stabilization by passive damping," *IEEE Trans. Power Electron.*, vol. 26. No. 7, pp. 1832-1836, Jul. 2011.

[8] X. Zhang and C. Mi, Vehicle Power Management: Modeling, Control and Optimization: Springer, 2011.

[9] Chris Mi, M. A. Masrur, and D. W. Gao, Hybrid Electric Vehicles: Principles and Applications with Practical Perspectives John Wiley & Sons Ltd, 2011.

[10] C. N. Onwuchekwa and A. Kwasinski, "Anlysis of boundary control for buck converters with instantaneous constant-power load," *IEEE Trans. Power Electron*., vol. 25. No. 8, pp. 2018-2032, Aug. 2010.

[11] J. Wang and D. Howe, "A power shaping stabilizing control strategy for dc power systems with constant power loads," *IEEE Trans. on Power Electron*., vol. 23, pp. 2982-2989, 2008.

[12] D. Feroldi, M. Serra, and J. Riera, "Energy Management Strategies based on efficiency map for Fuel Cell Hybrid Vehicles," *Journal of Power Sources*, vol. 190, pp. 387-401, 2009.

[13] D. J. Lee and L. Wang, "Small-signal stability analysis of an autonomous hybrid renewable energy power generation/energy storage system part I: Time-domain simulations," *IEEE Trans. on Energy Conv*., vol. 23, pp. 311-320, 2008.

[14] M. Zandi, A. Payman, J. P. Martin, S. Pierfederici, B. Davat, and F. Meibody-Tabar, "Energy management of a fuel cell/supercapacitor/battery power source for electric vehicular applications," *IEEE Trans. on Veh. Technol*., vol. 60, pp. 433-443, 2011.

[15] P. Liutanakul, A. B. Awan, S. pierfederici, B. Nahid-Mobarakeh, and F. Meibody-Tabar, "Linear stabilization of a DC bus supplying a constant power load: A General Design Approach," *IEEE Trans. Power Electron*., vol. 25 No. 2, pp. 475 - 488 Feb. 2010.

[16] X. Feng, J. Liu, and F. C. Lee, "Impedance specifications for stable DC distributed power systems," *IEEE Transactions on Power Electronics*, vol. 17, pp. 157-162, 2002.

[17] E. Jamshidpour, B. Nahid-Mobarakeh, P. Poure, S. Pierfederici, and S. Saadate, "Distributed stabilization in DC hybrid power systems," in *IEEE Vehicle Power and Propulsion Conf.*, VPPC Chicago,IL, USA, 2011.

[18] T. Boileau, B. Nahid-Mobarakeh, and F. Meibody-Tabar, "Back-EMF based detection of stator winding inter-turn fault for PM synchronous motor drives," in *Proceedings of the IEEE Vehicle Power and Propulsion Conf. VPPC*, Arlington, TX, 2007, pp. 95-100.